INSTITUTE OF PHYSICS PUBLISHING JOURNAL OF PHYSICS D: APPLIED PHYSICS
J. Phys. D: Appl. Phys. **36** (2003) R151–R165 PII: S0022-3727(03)26928-X

TOPICAL REVIEW

Relativistic laser–plasma interactions

Donald Umstadter

Center for Ultrafast Optical Science, University of Michigan, Ann Arbor, MI 48109, USA

E-mail: dpu@umich.edu

Received 19 November 2002
Published 2 April 2003
Online at stacks.iop.org/JPhysD/36/R151

Abstract

By focusing petawatt peak power laser light to intensities up to $10^{21}\,\mathrm{W\,cm^{-2}}$, highly relativistic plasmas can now be studied. The force exerted by light pulses with this extreme intensity has been used to accelerate beams of electrons and protons to energies of a million volts in distances of only microns. This acceleration gradient is a thousand times greater than in radio-frequency-based accelerators. Such novel compact laser-based radiation sources have been demonstrated to have parameters that are useful for research in medicine, physics and engineering. They might also someday be used to ignite controlled thermonuclear fusion. Ultrashort pulse duration particles and x-rays that are produced can resolve chemical, biological or physical reactions on ultrafast (femtosecond) timescales and on atomic spatial scales. These energetic beams have produced an array of nuclear reactions, resulting in neutrons, positrons and radioactive isotopes. As laser intensities increase further and laser-accelerated protons become relativistic, exotic plasmas, such as dense electron–positron plasmas, which are of astrophysical interest, can be created in the laboratory. This paper reviews many of the recent advances in relativistic laser–plasma interactions.

1. Introduction

Ever since lasers were invented, their peak power and focus ability have steadily increased. The most recent increases in power have been enabled by new techniques to produce shorter pulses. For instance, solid-state lasers use the technique of chirped-pulse amplification (CPA) [1, 2] to generate femtosecond duration pulses. To accomplish this, a laser pulse is first stretched in time before it is amplified and then recompressed. Gas lasers using solid-state switches have produced picosecond duration pulses [3]. Advanced laser systems now have multi-terawatt peak powers and, when focused to micron spotsizes with adaptive optics, can produce electromagnetic intensities $I \simeq 10^{21}\,\mathrm{W\,cm^{-2}}$, as illustrated by figure 1. Such intensities create novel states of matter, which are just beginning to be explored. For instance, electrons oscillate at relativistic velocities in laser fields that exceed $10^{11}\,\mathrm{V\,cm^{-1}}$, which results in relativistic mass changes exceeding the electron rest mass. At this point, the magnetic field of the electromagnetic wave also becomes important. Electrons behave in such fields as if the light wave was rectified. The propagation of light also depends in this regime on the light intensity, resulting in nonlinear effects analogous to those studied with conventional nonlinear optics—self-focusing, self-modulation, harmonic generation, and so on. Thus, a new field of nonlinear optics, that of relativistic electrons, has begun, as illustrated by figure 2. Rapid advancement in our understanding is underway and new research tools, subfields and commercial products are on the horizon, e.g. compact and ultrashort pulse duration laser-based electron accelerators and x-ray sources.

At the next physical regime that will be encountered at even higher intensities ($I \simeq 10^{24}\,\mathrm{W\,cm^{-2}}$), even protons will quiver relativistically. In this strongly relativistic regime of laser–plasma interactions, even more copious fusion and fission reactions and the generation of pions, muons and neutrinos should occur as energetic nuclei collide.

Discussed in this review are some of the latest highlights in high-field science, with greater emphasis given to experimental results. See also past reviews on relativistic nonlinear optics [4–6], high-intensity laser development [2], laser accelerators [7] and intense laser–plasma interactions [8–13]. Part of the discussion of the results obtained prior to the year 2000 first appeared in [5]. The paper is organized as follows: in

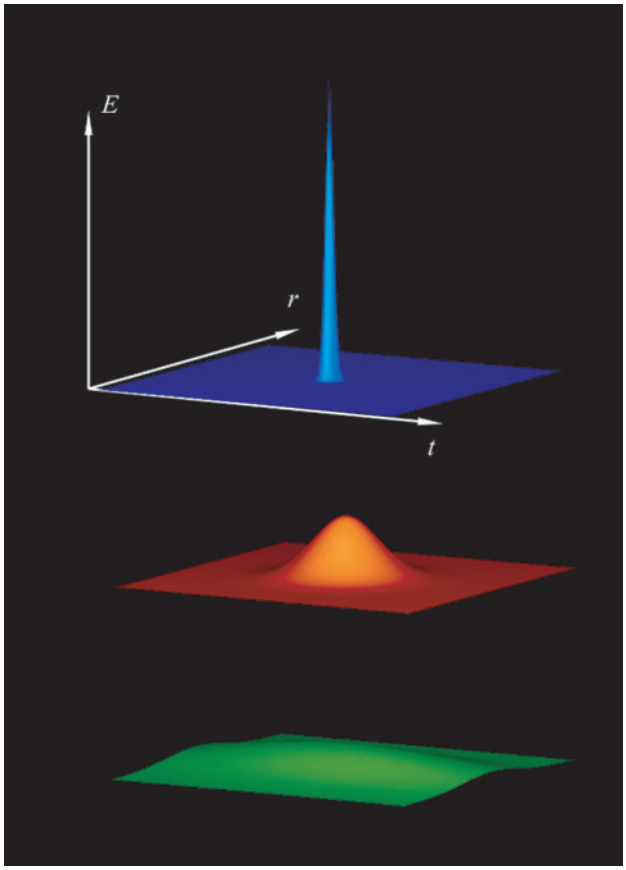

Figure 1. Laser light has become concentrated to ever-smaller regions of space (r) and time (t), dramatically increasing the peak electric field (E) at the laser focus. Prior to the development of CPA, the energy of light was produced in long-duration pulses, as shown in the green pulse of the bottom figure. After CPA, the pulse duration decreased dramatically as shown in the red pulse in the middle. The latest improvement in laser technology has been the use of deformable mirrors, which has allowed lasers to be focused to a spatial dimension that is as small as the temporal dimension, a few laser wavelengths, as shown in the blue pulse on top.

section 2, a brief basic theoretical overview of relativistic laser–plasma interactions is presented; detailed theoretical and numerical results are given in section 3.1, experimental results in section 3.2 and prospects and applications are reviewed in section 4.

2. Basic physical concepts

The interaction physics can be divided into two categories, which are differentiated by the density of the target used. In an underdense plasma, a low-intensity laser pulse would be transmitted through the plasma, while in an overdense plasma, it would be reflected. Atmospheric density gas jet are typically used as targets in the former case, while solid-density films or slabs are used in the latter case.

2.1. Gaseous-density targets

2.1.1. Electron quiver motion. Various physical regimes are encountered as the intensity of light is increased. At low light intensity, atomic electrons oscillate linearly, at the same frequency as the laser itself ($\omega = 2\pi c/\lambda = ck$). At higher field strengths, electrons become stripped from the atoms, i.e. the gas becomes ionized by tunnelling or multiphoton ionization. Linear perturbation theory can no longer be applied when the work done by the laser field on an electron (eEr_0) over the distance of the Bohr radius (r_0) approaches the Coulomb binding energy (e^2/r_0). At even higher intensities, electrons in the plasma that is formed will quiver at velocities close to the speed of light (c). Thus, the relativistic electron mass will increase and the $v \times B$ force in the Lorentz equation of motion (equation (1)), will become important.

$$F = \frac{\mathrm{d}(\gamma p)}{\mathrm{d}t} = eE + e\left(\frac{v}{c} \times B\right) \qquad (1)$$

In the relativistic regime, the quiver momentum of the electrons, p_0, exceeds m_0c, where m_0 is the electron rest mass and c is the speed of light. The parameter that sets the scale is a_0, the normalized vector potential, defined as $a_0 = p_0/m_0c = eE/m_0\omega c$, where e is the electron charge and E and ω are the electric field amplitude and the frequency of the laser light, respectively. In terms of other commonly used units, $a_0 = 0.85 \times 10^{-9}\sqrt{I}\lambda$, where I is the intensity of the laser light in W cm^{-2} and λ is the wavelength of the laser light in microns. When $a_0 \simeq 1$, which is satisfied for 1 μm light at a laser intensity of $\sim 10^{18}$ W cm^{-2}, the electron mass m_e begins to change significantly compared to the electron rest mass. (This relativistic regime was first approached as early as the late 1970s with large CO_2 lasers operated at 10 μm wavelength and intensities of 10^{15} W cm^{-2}, corresponding to $a_0 \simeq 0.3$ [14].)

For low fields, the solution to equation (1), is an electron motion described by an oscillation at the laser frequency along a straight line parallel to the polarization vector. For high fields, it is described by an average drift in the direction of laser propagation $\hat{k}$ and—in a frame that moves with the drift velocity—a figure-eight lying along the plane defined by the polarization vector and $\hat{k}$. The drift motion originates from the fact that $v \times B \propto E^2\hat{k}$. As the field strength increases ($a_0^2 \gg 1$), the longitudinal drift motion ($\propto a_0^2$) begins to dominate the transverse motion ($\propto a_0$), as shown in figure 3.

Since the motion is periodic, electrons that move in these figure-eight patterns should radiate photons that are harmonics of each other, with each harmonic having its own unique angular distribution (see figure 4). This is referred to as nonlinear Thomson scattering or relativistic Thomson scattering, predicted over 60 years ago [15]. If the electrons from which the light is scattered are initially in a directed beam, then the scattered light will be upshifted by an additional amount due to the relativistic Doppler shift, by a factor of $4\gamma^2$ (where γ is the relativistic Lorentz factor associated with the electron's velocity), which for electrons accelerated to 30 MeV corresponds to a factor of 10 000. Thus a 1 eV photon can be upshifted to 10 keV (illustrated in figure 5).

At even higher intensities, when the work done by the laser electric field over a distance of a Compton wavelength ($\lambda_C \equiv h/mc$) equals the rest mass of an electron, m_0c^2, pair production from the Dirac Sea will occur. The required value of E_0 is 6×10^{15} V cm^{-1}, corresponding to $I = 5 \times 10^{28}$ W cm^{-2}, which is a billion times higher than currently achievable. The observation of a statistically significant number of pairs is predicted to occur at somewhat lower fields, $E_0 \sim 10^{14}$ V cm^{-1} [16].

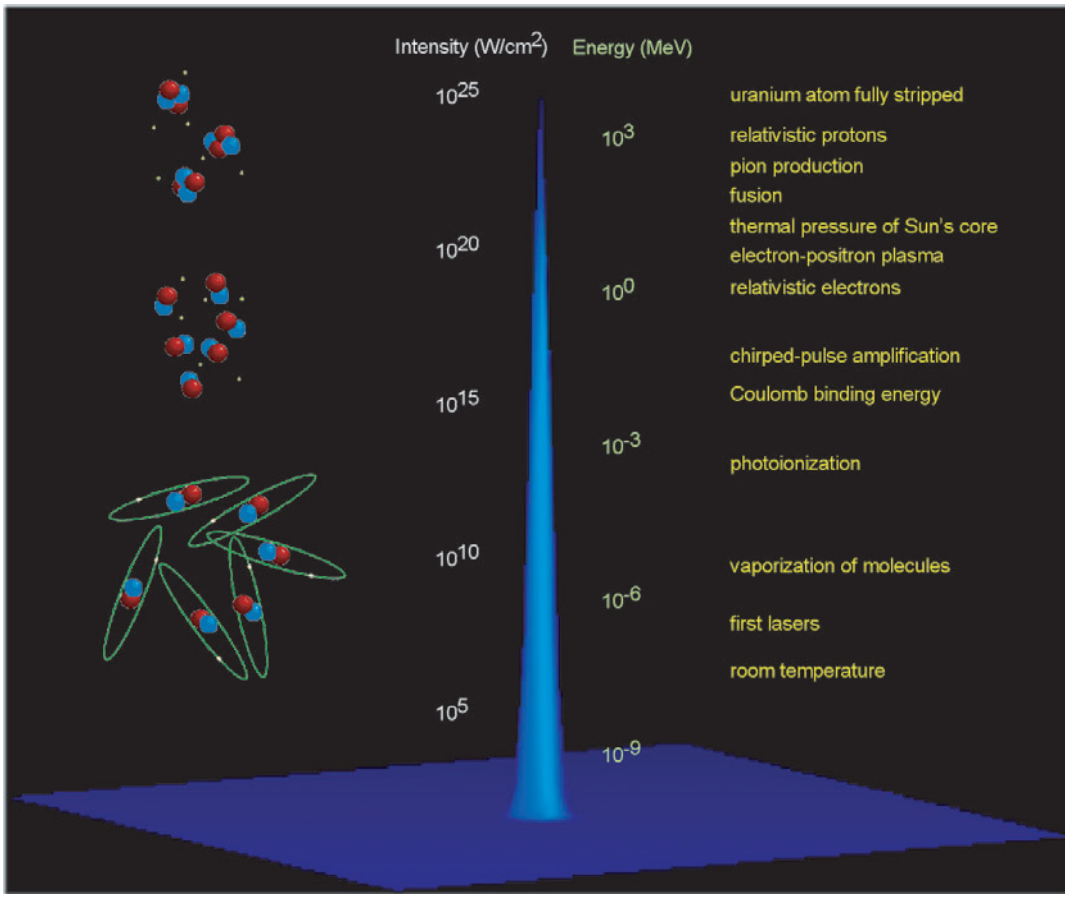

Figure 2. The various regimes of laser–matter interactions, represented by the ideal laser pulse. As the intensity of laser light increases, so does the energy of electrons accelerated in the light field and the regime of conventional nonlinear optics with electrons bound to atoms is replaced by the regime of relativistic nonlinear optics with free electrons in relativistic plasmas. At the highest intensities, even protons become relativistic, giving rise to what might be called the regime of nuclear optics, in which various nuclear processes, such as fusion, can take place.

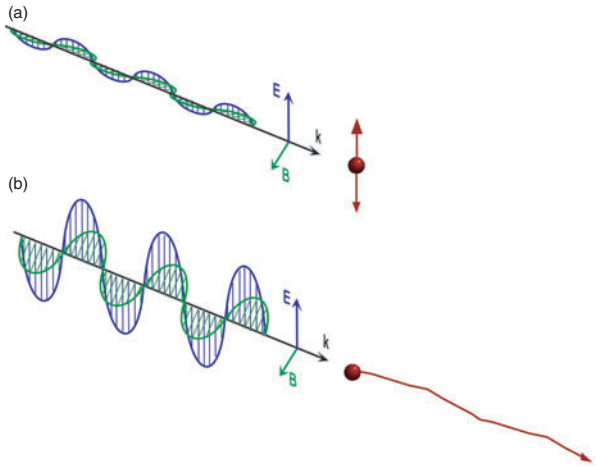

Figure 3. Classical optics versus relativistic optics. (*a*) In classical optics, the amplitude of the light wave is small, electrons oscillate in the direction of the electric field at the light's frequency and there is no displacement along the light's propagation direction. Note that only the E field acts on the electron, and the electron-oscillation velocity is very small compared with the speed of light. (*b*) In relativistic optics, the amplitude of the light wave is very large, the light's magnetic field becomes important and the combined action of the electric and magnetic fields pushes the electron forward. In this case, the electron velocity becomes close to the speed of light.

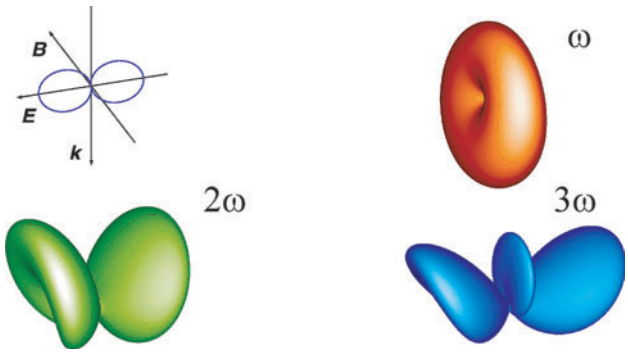

Figure 4. Harmonics driven by relativistic Thomson scattering as the electrons in high-intensity laser fields ($a_0^2 \sim 1$) undergo figure-eight motion display unique angular distributions.

2.1.2. Collective effects. At high laser intensity, the relativistic change in the electron mass alters the plasma frequency, $\omega_p = \omega_{p0}/\gamma^{1/2} = (4\pi n_e e^2/\gamma m_0)^{1/2}$, where ω_{p0} is the plasma frequency in a quiescent plasma, e is the electron charge, m_0 is the electron rest mass, n_e is the plasma electron density and $\gamma = \sqrt{1 + a_0^2}$ is the relativistic Lorentz factor. This in turn alters the dielectric properties of a plasma medium through the modification of the index of refraction

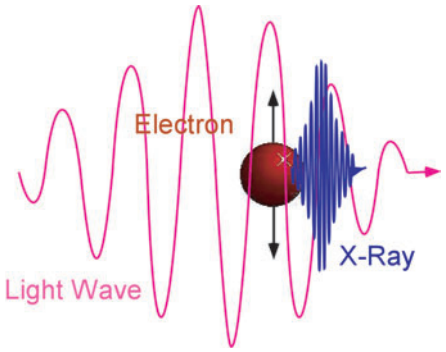

Figure 5. Harmonic generation and a relativistic Doppler shift can up-shift the frequency of visible radiation from a laser that Compton scatters from an energetic electron beam to the x-ray region of the spectrum. Colliding a laser with 100 MeV energy electron beams from a tabletop laser accelerator can produce 50 keV x-rays, which are useful for atomic scale metrology with femtosecond temporal resolution and medical imaging.

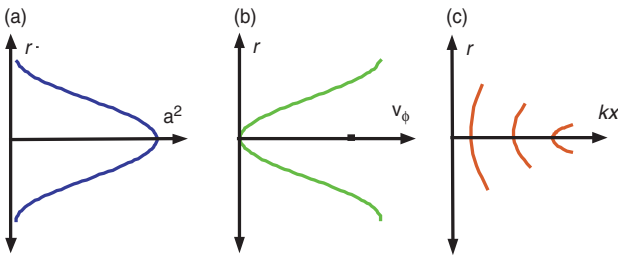

Figure 6. The mechanism of relativistic self-focusing. (*a*) An on-axis peak in laser intensity (a^2) for a Gaussian pulse produces greater electron quiver motion on axis than off axis. (*b*) The phase velocity of light (v_ϕ) depends inversely on the laser intensity via the change in the index of refraction, which depends on the relativistic electron mass. (*c*) Variation of the phase velocity with radius causes the wavefronts to curve inward as the pulse propagates, focusing the light as with a positive lens.

of the light wave, given by $\eta = [1 - (\omega_p/\omega)^2]^{1/2}$. If there is an on-axis maximum of the radial profile of γ, such as is created by a laser beam with an intensity profile peaked on axis, as shown in figure 6, or $\gamma(0) > \gamma(r)$, then the index of refraction, $\eta(r)$, can have a maximum on axis. By causing the wavefront to curve inward and the laser beam to converge, this will result in optical guiding of the laser light. Since the laser phase velocity v_ϕ depends on the index of refraction, $v_\phi = c/\eta$, it will then depend on the laser intensity. Local variation in the phase velocity will modify the shape of the laser pulse, and, consequently, the spatial and temporal profile of the laser intensity. Relativistic self-focusing occurs when the laser power exceeds a critical power, given by $P_c = 17(\omega_0/\omega_p)^2$ GW. On the other hand, photo-ionization can defocus the light and thus increase the self-focusing threshold, by increasing the on-axis density and refractive index. When this focusing effect just balances the defocusing due to diffraction, the laser pulse can be self-guided, or propagate over a long distance with high intensity.

2.1.3. Light pressure. Not only can the plasma affect the light, but the light can affect the plasma. Electrons are pushed to regions of lower light intensity by the ponderomotive force, which for $a_0 \ll 1$ is proportional to the gradient of the light pressure, $\nabla P \propto \nabla(n_e I\lambda^2)$, or the time-averaged quiver energy density, $P = n_e(\gamma - 1)m_0c^2$. A Gaussian-shaped laser intensity profile will tend to expel electrons radially from the axis, often referred to as 'electron cavitation'. Eventually, the charge displacement due to expelled electrons will move the ions, forming a channel with a density depression on axis, $n_e(0) < n_e(r)$. Again, $\gamma(0) > \gamma(r)$ results, enhancing relativistic self-guiding or allowing a second trailing laser pulse to be guided. Such density channels have also been created by a thermal gradient, which was produced by a long-duration laser pulse, or by means of a capillary discharge.

It is obvious that the interplay between modulations of the light intensity, ponderomotive modulations of the plasma density, modulations of the index of refraction and eventually further modulations of the light intensity, can lead to instabilities, such as self-modulation and Raman scattering.

2.1.4. Electron acceleration. The light-pressure driven density modulations just discussed can drive large amplitude plasma waves. The growth rates depend on the duration of the light pulse relative to the plasma period. For underdense plasmas and the short pulse durations that are required to produce high laser intensity, there is not enough time for ions to move significantly compared to electrons. A local charge displacement results when the electrons are pushed by the light pressure. The electrostatic restoring force causes the plasma electrons to oscillate at the plasma frequency (ω_p), creating alternating regions of net positive and negative charge. An electrostatic wakefield plasma wave results, which propagates at a phase velocity nearly equal to the group velocity of the light pulse, which can be close to the speed of light for low-density plasmas. A relativistic electron can then be continuously accelerated. Remarkably, the acceleration gradient (200 GeV m^{-1}) can be four orders of magnitude larger than in conventional rf linacs (<20 MeV m^{-1}) [7]. A plethora of methods have been proposed for driving such plasma waves [7], including the plasma beat-waves [17], laser wakefields (LWFA) [17], tailored pulse trains [18], and the self-modulated laser wakefields (SMLWFA) [19–21].

Of these approaches, laser beatwaves were first to be demonstrated [22, 23] because long-pulse medium-power lasers were developed 30 years ago. More recently, with the development of short-pulse high-intensity lasers, the LWFA and the SMLWFA were demonstrated. In the LWFA, an electron plasma wave is driven resonantly by a short laser pulse ($\tau \sim \tau_p$) through the laser ponderomotive force (see figure 7). In the resonant laser plasma accelerator, a train of Gaussian-shaped pulses with variable durations and inter-pulse spacings can stay in resonance with a wakefield as it grows nonlinearly [18]. In the SMLWFA, an electromagnetic wave ($\omega_0, \boldsymbol{k}_0$) decays into a plasma wave ($\omega_p, \boldsymbol{k}_p$) and another forward-propagating light wave ($\omega_0 - \omega_p, \boldsymbol{k}_0 - \boldsymbol{k}_p$) via the stimulated Raman forward scattering instability. In this case, the laser pulse duration is longer than an electron plasma period, $\tau \gg \tau_p = 2\pi/\omega_p$.

In order to produce a high quality beam of relativistic electrons, electrons need to be injected into the appropriate phase of the plasma wave in any of these laser-based accelerators. That beam can be provided by an external electron gun or produced in the plasma itself. Electrons can be uncontrollably heated by acceleration in Raman backscattered

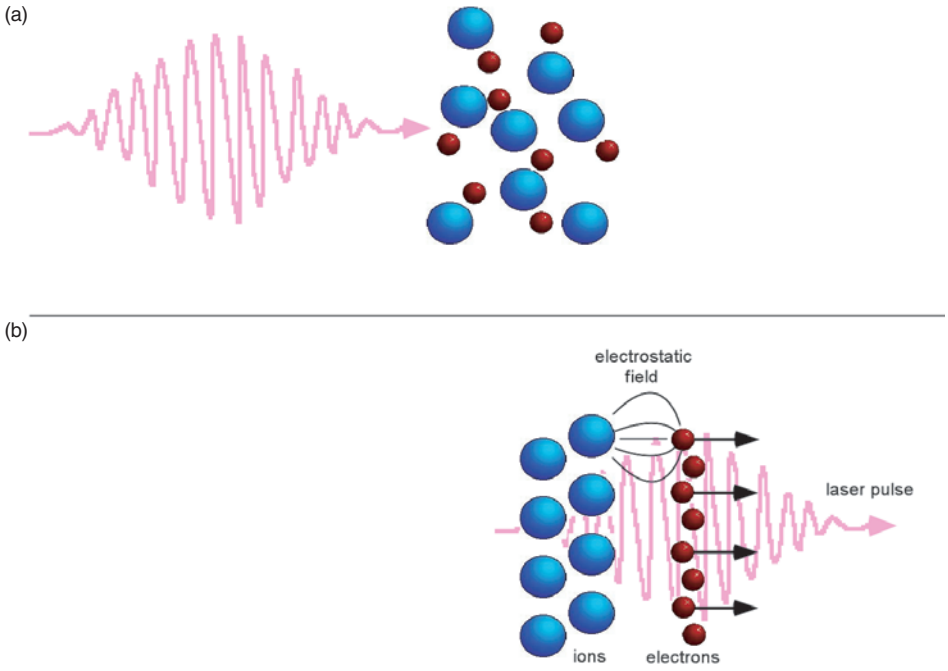

Figure 7. The laser wakefield mechanism. (*a*) A laser pulse interacts with a plasma, an ionized gas, composed of electrons and ions. (*b*) In the relativistic regime, the electromagnetic force acting on the electron pushes the electrons forward in the laser direction. The charge separation between the light electrons and the massive ions in a plasma produces a large longitudinal static electric field comparable to the transverse field of the laser. Note that the plasma acts as an efficient optical rectifier.

plasma waves and sidescattering instabilities [24–26] or by wave-breaking (longitudinal [7] or transverse [27]). These electrons can become trapped in the fast wakefield plasma wave, but will produce a beam with a large energy spread. On the other hand, the characteristics of the generated electron beam can be controlled by proposed injection schemes [28–33, 211], in which all of the plasma electrons that become trapped (in the acceleration bucket of the fast plasma wave) have the same phase. Besides compact size, another advantage of an all optically driven plasma-cathode electron gun is absolute synchronization between the electrons and laser for pump and probe experiments in ultrafast science.

2.1.5. Self-generated magnetic fields. The large (kiloampere) currents that are produced by laser-accelerated electron beams can induce large poloidal magnetic fields [34]. A circularly polarized light beam can generate an axial magnetic field [35] by inducing current loops via the inverse Faraday effect. If there is a temperature gradient orthogonal to a density gradient, then the thermoelectric effect can also induce a toroidal field. In all of these cases, megaGauss, even gigaGauss field strengths can be driven.

2.2. Solid-density targets

Low-intensity laser light cannot normally propagate into overdense plasma, above the critical density, n_c, defined by the density at which $\omega = \omega_p$. Thus, different physics is encountered when a solid-density target is used.

2.2.1. Proton acceleration. When electrons are heated to high temperatures or accelerated to high energies, they can separate from plasma ions. Such charge displacement creates an electrostatic sheath, which eventually accelerates the ions. The ions are pulled by the charge of the electrons and pushed by the other ions' unshielded charges (similar to the 'Coulomb explosion' that can occur during the ionization of atoms). When the charge displacement is driven by thermal expansion, as in long-pulse (low power) laser–plasma experiments, the maximum ion energies are limited to less than 100 keV. However, when the charge displacement is driven by direct laser heating, as in short-pulse high-power laser–plasma experiments, multi-megaelectronvolt ion energies are possible. This was first shown with gas jet targets [137, 136], in which case the ions were accelerated radially into 2π, and then later with thin solid-density-films [138–140], in which case the ions were accelerated into collimated beams. In the latter case, hydrocarbons and water on the surface of the film can become ionized and provide a source of protons to be accelerated.

An intense laser can ponderomotively heat electrons. If the laser contrast is high, vacuum heating can occur in the following manner. When light encounters a sharp interface between vacuum and solid density, the electromagnetic field becomes evanescent in the region above the critical density. The instantaneous '$v \times B$' force can push electrons in the direction of the light's propagation vector; it also has a frequency twice that of the pump and a magnitude proportional to the square of the normalized vector potential, a_0^2. Thus electrons can only complete half of their figure-eight orbits, on the vacuum side, gaining relativistic energies [36]; they move through the overdense region without the electromagnetic field to pull them back. An electrostatic sheath can thus form, which will accelerate the ions left behind. Another important heating mechanism is stochastic heating [70, 150], which occurs when the light that is reflected from the critical surface beats with

the incoming wave to create a standing wave. The motion of electrons in such a wave can become chaotic, resulting in a large increase in electron temperature (>100 keV).

As the heated electrons propagate through a solid, they can instantaneously field-ionize the neutral atoms of the solid. This will both modify the solid's conductivity and provide a source of protons on the rear-side of the target. If the film is thin enough, the electrons can pass through, and create a sheath on the rear-side of, the target. This latter mechanism has been dubbed the target normal sheath acceleration (TNSA) mechanism. The ions from thin foils have been claimed to originate from both the front and rear-side of the foil.

2.2.2. Critical surface interactions. The $v \times B$ term of equation (1) oscillates at 2ω because it is a product of two sinusoidal terms oscillating at ω. Thus, the critical surface (the location of the critical density) where the light is reflected, can also oscillate at 2ω. Frequency mixing can then produce harmonics in solid-target experiments, as has been observed since the early days of intense laser interactions (with CO_2 lasers) [37].

As discussed above, relativistic mass shifts can change the plasma frequency. This will act to shift the critical-density to higher values for a fixed incident laser frequency, inducing transparency of even solid targets by intense pulses. The pressure of intense laser pulses can also push the critical surface towards the solid-density region [38, 39], or also push plasma sideways in a process called 'hole-boring' [40].

3. Recent findings

3.1. Analytical and numerical

Most of all the phenomena discussed in section 2 have been extensively studied with analysis and numerical simulation. The nonlinear regime ($a_0^2 \gg 1$) of intense laser interactions with underdense plasma is very well understood theoretically assuming one dimension, or the laser spotsize is much greater than the plasma wavelength. This includes nonlinear plasma waves, wavebreaking, quasi-static laser propagation, nonlinear growth rates for instabilities and harmonic generation. Numerous fluid, particle, and Vlasov codes are also valid in this approximation. Many of the same phenomena are also understood in three dimensions, but only in the linear regime ($a_0^2 \ll 1$).

3.1.1. Propagation, plasma wave generation and acceleration in underdense plasma. There has been some progress in the three-dimensional nonlinear regime. For instance, there exists a unified cold-fluid-Maxwell model treatment of electron parametric instabilities, assuming a one-dimensional plane-wave high-intensity pump laser field [41, 42]. Novel effects, such as the coupling of forward Raman and self-modulation instabilities, including the effects of a radially bounded pump laser field, have also been analysed [43, 44]. Collisional absorption when the plasma temperature is nonrelativistic and the electron quiver velocity is fully relativistic has been discussed [45]. The production of electron–positron pairs by the interaction of relativistic superthermal electrons generated by ultraintense laser pulses with high-Z material has been considered [46]. It is found that when the pairs are sufficiently confined, they can start to exponentiate in number, achieving a pair density approaching $10^{21}\,\mathrm{cm}^{-3}$. Several authors have studied the acceleration of electrons directly from the laser field in vacuum [47, 48].

Much progress has also been made in this regime through simulations. Although very demanding computationally, three-dimensional full-scale particle-in-cell simulations solve Maxwell's equations and the equation of motion, equation (1), without approximation for each particle simultaneously. The VLPL was an early example, which can run on a massively parallel computer CRAY-T3E with 784 processor elements. It uses up to 10^9 particles and 10^8 grid cells and was used to study relativistic self-focusing and cavitation [49], and later hole-boring [50]. Coalescence of two laser-beam filaments into a single filament was observed and thought to be due a self-generated magnetic field. Another three-dimensional PIC code, which is fully explicit, object-oriented and parallelized is OSIRIS. It was used to observe the formation of a braided pattern due to the mutual attraction of two co-propagating laser beams in a plasma [51]. The mechanism is similar to self-focusing, discussed in section 2.1.1, except the one filament modified the index of refraction seen by the other filament. The magnetic field of a plasma wake driven by laser pulse has also been studied [52].

A three-dimensional PIC code was used to study the propagation of an intense pulse through an underdense plasma, showing the formation of a 'shock' on the front of the pulse, ion filaments and double layers [32]. The amplitude of the circularly polarized laser was $a_0 = 50$, the mass ratio was $m_\mathrm{p}/m_\mathrm{e} = 1840$, and $\omega_\mathrm{p}/\omega = 0.45$. A three-dimensional version of the VLPL code has been used to investigate electron acceleration by the inverse-free-electron-laser mechanism [53]. Electrons propagating in a plasma channel can execute betatron oscillations from the self-generated static electric and magnetic fields. If the power of the laser greatly exceeds the threshold for relativistic self-focusing and the betatron oscillations are in resonance with the light pulse's electric field, then the electrons can gain energy directly from the laser. The results of a simulation of electron acceleration from an underdense target were used to support the argument that most of the energy acquired in a real experiment conducted under similar conditions [54] is due to direct laser acceleration, while laser wakefield acceleration (LWFA) drives only a minority of electrons.

Another code that has been used to study wakefield generation and laser propagation in the limit $a^2 \ll 1$ is named SIMLAC [55, 197]. It follows the motion of the pulse in its group velocity frame. When this code was used to study wakefields, the laser pulse and wake were observed to be maintained over long enough propagation distance to accelerate an electron to gigaelectronvolt energy.

A three-dimensional envelope equation for the laser field was derived analytically, which includes nonparaxial effects, wakefields, and relativistic nonlinearities [197]. In the broad beam, short pulse limit the nonlinear terms in the wave equation that lead to Raman and modulation instabilities cancel. Tapered plasma channels are found to increase the dephasing length and thus the final accelerated electron energy [205, 199]. A two-dimensional envelope model that does not

make the paraxial approximation, and thus allows for a wave with a finite group velocity, has been used to model self-modulation. It is found to reduce the growth rate of the SMLWFA [43]. It was found that in the very-underdense-plasma limit, a separation of the ω and ω_p timescales need not be assumed in a Maxwell-fluid model [56]. Rather than having to grow from noise, the perturbation from which Raman forward scattering can grow can be seeded by either ionization fronts or Raman backscatter [201]. Plasma wakes can also be excited by colliding long and short pulse duration counter-propagating laser beams [210]. This is related to a method by which the wakefield of one ultrashort laser pulse is amplified by a second co-propagating laser pulse [207]. A mechanism that leads to efficient acceleration of electrons in plasma by two counterpropagating laser pulses was proposed [209]. It is triggered by stochastic motion of electrons when the laser fields exceed some threshold amplitudes, as found in single-electron dynamics. It is further confirmed in particle-in-cell simulations.

Tricks have been suggested to get around the Lawson–Woodward criteria, which limits the means by which electrons can be accelerated in vacuum. For instance, using three-dimensional test particle simulations, the characteristics and essential conditions under which an electron in a vacuum laser beam can undergo a capture and acceleration [212] have been examined. When $a_0 \leqslant 100$, the electron can be captured and violently accelerated to energies $\geqslant 1$ GeV with an acceleration gradient $\geqslant 10\,\mathrm{GeV\,cm^{-1}}$. Classical fifth order calculations in the diffraction angle show that electrons, injected sideways into the tightly focused petawatt-power laser beam, get captured and gain energy in the gigaelectronvolt regime [205].

A multiple timescale expression for the ponderomotive force of an intense light pulse has also been proposed [57]. The generation of forward Raman radiation shifted by half the plasma frequency, for laser intensities of order or exceeding $10^{18}\,\mathrm{W\,cm^{-2}}$, has recently been predicted [58]. It has been observed in PIC-code simulations that self-focusing and ponderomotive blow-out can be suppressed by the occurrence of Raman scattering and plasma heating [59]. It has been shown theoretically that non-Gaussian-shaped pulses can drive wakefields more effectively than Gaussian-shaped pulses [60]. Similar improvements might be obtained by the use of pulse shapes that are more easily produced experimentally using a genetic algorithm [61]. The behaviour of the electron beam that is accelerated in a plasma wave has been studied with several PIC and test-particle simulations [24, 62–67].

3.1.2. Acceleration from solid-density targets. The acceleration of electrons and ions from solid targets, which was described in section 2.2.1 has been studied extensively with PIC simulations. As an example, protons with a maximum energy of 40 MeV and electron and proton densities of $10^{21}\,\mathrm{cm^{-3}}$ were observed with a three-dimensional PIC code [68]. Another PIC simulation showed that those protons emitted from the back side occupy a narrower longitudinal velocity phase space than those that come from the front side [69]. A thin foil target shaped like a hemisphere so that the field lines would converge on axis produced a low-emittance proton beam [70, 148]. The angular distributions of fast electrons, ions, and bremsstrahlung x-rays were also studied [208, 71]. A simulation shows that stochastic heating of electrons in the beating of the incident and reflected wave heats the electrons to multi-megaelectronvolt energies and accelerates them into the dense plasma, where, at the rear surface of the dense plasma (but the front of the target), they accelerate the ions into the target [**?**]. Another simulation shows the focusing of fast protons created in the interaction of laser radiation with a spherical target is possible with the focal spot of fast protons near the centre of the sphere. The conversion efficiency of laser energy into fast ion energy attains 5% [151]. Both front and backside ion acceleration and a 10 MG magnetic field are observed in simulations of an intense laser ($10^{19}\,\mathrm{W\,cm^{-2}}$ and 150 fs) interacting with a solid-density thin film [152].

3.1.3. Nonlinear scattering and harmonic generation. Although much of the theoretical analysis of nonlinear Thomson scattering was originally done in the 1960s, several refinements have been published only recently.

The production of harmonics by nonlinear Raman backscattering mechanism has been reanalysed [95] using the wave equation and fluid equations instead of relying on analysis of free electrons. The backscatter is found to occur at odd multiples of the Doppler-shifted pump frequency (for the case of an electron beam). The effects of stimulated Raman scattering on radiation generation has also been explored [94]. It shows that for maximal growth rate a high level of spectral purity in the electron beam is required.

Relativistic harmonic generation in a plasma is considered by determining a current density based on the relativistic Lorentz equations [87]. Maxwell's equations are used to solve for harmonic generation, and this solution shows oscillation in the strength of the harmonic. Resonant density modulation of the plasma through an ion acoustic wave is shown to allow for linear growth of the harmonic.

A complete three-dimensional theory of Compton scattering is described [96], which fully takes into account the effects of the electron beam emittance and energy spread upon the scattered x-ray spectral brightness. The radiation scattered by an electron subjected to an arbitrary electromagnetic field distribution in vacuum is first derived in the linear regime and in the absence of radiative corrections. It is found that each vacuum eigenmode gives rise to a single Doppler-shifted classical dipole excitation. This formalism is then applied to Compton scattering in a three-dimensional laser focus, and yields a complete description of the influence of the electron beam phase-space topology on the x-ray spectral brightness; analytical expressions including the effects of emittance and energy spread are also obtained in the one-dimensional limit. Within this framework, the x-ray brightness generated by a 25 MeV electron beam is modelled, fully taking into account the beam emittance and energy spread, as well as the three-dimensional nature of the laser focus; application to x-ray protein crystallography is outlined. Finally, coherence, harmonics, and radiative corrections are also briefly discussed.

The Thomson scattering spectrum of an electron by an ultraintense laser field has been computed. It is found that the electron orbit—and therefore its nonlinear Thomson scattering spectra—depend critically on the amplitude of the ultraintense laser field and on the phase at which the electron sees the laser electric field. Contrary to some customary notions,

the harmonics of Thomson scattering spectra, in general, do not occur at integer multiples of the laser frequency, and the maximum frequency is proportional to the first instead of the third power of the electric field strength [82, 83].

A charged particle in circular orbit at relativistic velocities will create short pulse radiation for an observer in the plane of rotation. If this radiation arises out of a source size smaller than a wavelength, we consider it coherent, because all secondary sources encounter the same phase from the incident laser. From scattering theory, coherent radiated power goes as the square of the source number; this however motivates a reconsideration of radiation reaction for the case of coherent scattering. Inclusion of this analysis is shown to result in an optimal number of electrons for maximum radiated energy [85]. Of course, even shorter pulses would be seen by particles of relativistic velocity directed along the plane of electron rotation. An additional benefit of the circular trajectory of the electrons is generation of an astronomically significant magnetic field at the centre of the rotation.

A scheme is proposed to create a single (as opposed to pulse train) 500 as, VUV pulse [84]. Citing the key requirement for short pulse radiation as a source size corresponding to a time spread less than the desired output, the authors propose using a tightly focused electron beam as the scattering medium. The proposed method capitalizes on the ponderomotive force originating from the spatial profile of the light to limit the electron scattering time to less than that of the original pulse. A co-propagating geometry of two pulses shifted in phase by one-half wavelength helps to homogenize the field seen by electrons along the direction of propagation.

The power, energy spectrum, brilliance, polarization and time structure of x-rays produced by Larmor and Bremsstrahlung radiation [93] were evaluated.

Radiation emitted by an electron in arbitrary, extreme relativistic motion has been described for the first time in terms of a standard spectrum of nonsynchrotron type [97]. Ultimately, such a nonsynchrotron spectrum is dependant not only on instantaneous trajectory curvature but also upon its first two time derivatives and helicity to provide a basic correction to the synchrotron approximation. A strong deviation has been predicted for above gigaelectronvolt electrons in oriented crystals.

A scheme for bright sub-100 fs x-ray radiation generation using small-angle Thomson scattering is proposed [91, 88, 83]. Coupling high-brightness electron bunches with high-power ultrafast laser pulses, radiation with photon energies between 8 and 40 keV can be generated with pulse duration comparable to that of the incoming laser pulse and with peak spectral brightness close to that of the third-generation synchrotron light sources.

PIC codes have also been used to study harmonics generated from critical-surface interactions. A normal incidence circularly polarized laser is predicted to generate harmonics with each order having a different characteristic angle [72–74]. A strong effect of radiation damping on the interaction of an ultraintense laser pulse with an overdense plasma slab is found and studied via a relativistic particle-in-cell simulation including ionization. Hot electrons generated by the irradiation of a laser pulse with a radiance of $10^{22}\,\mathrm{W\,cm^{-2}}$ and duration of 20 fs can convert more than 35% of the laser energy to radiation [100]. This incoherent x-ray emission lasts for only the pulse duration and can be intense. The radiation efficiency is shown to increase nonlinearly with laser intensity. Similar to cyclotron radiation, the radiation damping may restrain the maximal energy of relativistic electrons in ultraintense-laser-produced plasmas.

3.1.4. Solitons and electromagnetic transparency. Two qualitatively different scenarios for the penetration of relativistically intense laser radiation into an overdense plasma, accessible by self-induced transparency, were investigated [75]. In the first one, penetration of laser energy occurs by soliton like structures moving into the plasma. This scenario occurs at plasma densities less than approximately 1.5 times critical (depending on ion mass). At higher background densities, laser light penetrates only over a finite length which increases with incident intensity. In this regime the plasma-field structures represent alternating electron and, on longer timescales, ion layers separated by about half a wavelength of cavitation with concomitant strong charge separation. With particle-in-cell simulations, electromagnetic, relativistically strong solitons, formed in the wake of the laser pulse during the interaction of a high-intensity ultrashort laser pulse with a collisionless plasma, are shown to evolve asymptotically into post-solitons [76]. A post-soliton is a slowly expanding cavity in the ion and electron densities which traps electromagnetic energy and accelerates ions upon formation. Post-solitons are elementary components of the relativistic electromagnetic turbulence in laser-irradiated plasmas. The ion motion influence on the relativistic soliton structure is investigated. In the case of moving multimode solitons, the effect of the ion dynamics results in the limiting of the soliton's amplitude [77]. The constraint on the maximum amplitude corresponds to either the ion motion breaking in the low-node-number case, or to the electron trajectory self-intersection in the case of high-node-number solitons. The soliton breaking leads to the generation of fast ions and provides a novel mechanism for ion acceleration in a plasma irradiated by high-intensity laser pulses.

3.2. Experimental

3.2.1. Relativistic electron motion, Thomson scattering and harmonic generation. One of the predictions of the fully relativistic analysis of the interaction of intense light with electrons is that the canonical momentum will be conserved. This prediction was clearly verified experimentally in studies of the angular distribution of relativistic electrons that are emitted from the barrier-suppression ionization of atoms [78]. The unique angular distributions of the second and third harmonics emitted from nonlinear relativistic Thomson scattering were observed experimentally [79]. The scaling of the harmonics with laser power and density confirmed that the emission was incoherent. Harmonic emission in the near-forward direction was observed in both the optical [80] and the XUV [81] spectral regions. In the latter case, the harmonic emission was attributed to scattering from the megaelectronvolt energy electron beam that was accelerated by the same laser pulse that was scattered, often described as Compton scattering.

The second-harmonic emission generated by spatially asymmetric quivering electrons caused by the ponderomotive force was studied [92]. The intensity of the second harmonic was proportional to the focused intensity of the pump pulse with the power of 1.8. This intensity dependence can be explained by the relativistic effect of the quivering electrons.

The generation of high harmonics created during the interaction of a 2.5 ps, 1053 nm laser pulse with a solid target has been recorded for intensities up to $10^{19}\,\mathrm{W\,cm^{-2}}$. Harmonic orders up to the 68th at 15.5 nm have been observed in first order diffraction with indications of up to the 75th at 14.0 nm using second-order [98]. No differences in harmonic emission between s and p polarization of the laser beam were observed. The power of the 38th high harmonic at 27.7 nm is estimated to be 24 MW. An experimentally measured increase in laser absorption was observed as the laser intensity is raised [99], which was attributed to vacuum heating, consistent with theoretical predictions [36].

The fact that the electric field in a frame moving with a relativistic electron beam is boosted by γ, where γ is the relativistic factor associated with electron beam, has allowed the observation of pair production from the vacuum with current laser technology [101,102]. Using the 30 GeV electron beam of the stanford linear accelerator, the field was increased by a factor of 5×10^4, and therefore in this case, the threshold for observation of pair-production was exceeded with a laser operating at an intensity of only $10^{19}\,\mathrm{W\,cm^{-2}}$.

3.2.2. Guiding. As discussed in section 2, self-guiding is possible when laser power exceeds the threshold for relativistic self-guiding, P_c. Various authors have reported the observation of relativistic self-guiding [103–108]. A second intense laser pulse has then been guided in such a preformed channel [109, 79]. The critical power for relativistic self-focusing P_c has been shown experimentally [190] not the only relevant parameter, particularly when the laser pulse duration is comparable to plasma particle timescales: ω_p^{-1} for electrons and Ω_p^{-1} for ions. Using time-resolved shadowgraphy, pulses are observed to not relativistically self-focus if the pulse duration is too short compared to ω_p^{-1}, even in the case where the power is greater than P_c. For pulses longer than ω_p^{-1}, self-focusing can occur even for powers lower than P_c. When channel extension was characterized via the Thomson-scattered light and the impact of the laser pulse duration and chirp were studied, the channel was seen to extend further when the pulse duration is increased under certain conditions [144].

Several authors have studied the propagation of intense pulses in preformed plasmas. Different regimes of propagation are observed when the pulse duration is varied [191]. The plasma wave is generated by either envelope self-modulation of the pulse or self-focusing and Raman instabilities. An axicon lens has been used to produce a density channel extending many Rayleigh lengths by means of thermal expansion driven by long-pulse channel-forming laser [110]. Such channels have been used to guide pulses of intensities reaching $10^{17}\,\mathrm{W\,cm^{-2}}$ in plasmas reaching densities of $10^{16}\,\mathrm{cm^{-3}}$. In order to take advantage of the uniformity of low-Z gases, such as helium and hydrogen, a spark discharge was used to seed breakdown [111]. Alternatively, channels can be formed by using two transversely injected laser pulses, as in the igniter–heater scheme [112]. Capillary discharges have been used to guide pulses, achieving 70% transmission of pulses with intensities reaching $10^{17}\,\mathrm{W\,cm^{-2}}$ over distances of up to 20 Rayleigh ranges [113]. An innovative technique for measuring the propagation of intense laser pulses through plasma channels is described [202]. At high laser intensities, temporally resolved stimulated Raman backscattering can be used to diagnose both the electron density and the laser intensity inside the plasma channel. Velocity control and staging of laser wakefield accelerators in segmented capillary discharges has also been investigated [200].

The observation of laser self-focused channel formation into overdense plasmas (hole-boring) has been reported in experiments making use of a soft x-ray laser probe system with a grid image refractometry technique. Cross sections of a 30-μm diameter channel were obtained that the authors attribute to hole-boring in overdense plasmas [114]. Hole-boring has also been investigated by means of transmission measurements [115].

3.2.3. Electron acceleration. Several groups have observed the acceleration of megaelectronvolt electrons by the SMLWFA [25, 26, 108, 120, 116–118], with a large energy spread. Most of the electrons have energies less than 5 MeV, with the number decaying exponentially and some electrons at energies up to 200 MeV [118]. While in an early paper, the electron acceleration was attributed to catastrophic wave-breaking of a relativistic Raman forward scattered plasma wave [120], this has more recently been attributed to the wavebreaking of a slower velocity Raman backscattered wave [25, 26]. Recently, a two-temperature distribution in the electron energy spectrum is reported [105], which was attributed to a combination of two different acceleration mechanisms: (1) directly by the laser field and (2) by the plasma wave. A two-temperature distribution was also observed in a different experiment [121], as well as a multi-component spatial profile of the electron beam, measured at a distance of 10 cm from the gas jet. Electrons in the low energy range were observed to undergo an abrupt change in temperature, coinciding with the onset of extension of the laser channel due to self-guiding of the laser pulse, when the laser power or plasma density was varied [108]. In contradiction to the theory that two mechanisms are responsible, these same features have been found in a simulation in which test electrons were injected into the self-consistent fields of a three-dimensional plasma wave (without the presence of a laser pulse) [121].

Electrons have also been observed to be accelerated beyond the linear dephasing limit, which was explained, using PIC simulations, to be the consequence of the electron-driven wakefields created by trapped electrons [122]. By imaging the electron beam as the laser power increases, the divergence angle of the electron beam is seen to decrease [121]. The lowest angle, 1°, obtained at the highest power, corresponds to a transverse geometrical emittance of $\epsilon_\perp \leqslant 0.06\pi$ mm mrad [121], which is an order of magnitude lower than that from the best conventional electron gun. This may be because a large acceleration gradient decreases the time over which space-charge can act to degrade the emittance. The production of ultracollimated bunches of multi-megaelectronvolt electrons

by a 35 fs laser pulse propagating in exploding-foil plasmas was studied [196]. Up to 10^9 electrons per shot were accelerated, most of which were in a beam of aperture below 10^{-3} sterad, with energies up to 40 MeV.

Several groups [123, 124] have measured the plasma wave amplitude as a function of time by means of collinear Thomson scattering and found that it decays in $\sim 50\tau_p$. By direct measurement of ion waves, the modulational decay instability (in which electron plasma waves decay into ion waves) has been shown to play an important role in the damping of plasma waves [125]. The longitudinal spatial profile of the plasma wave has been measured by means of coherent Thomson side-scattering. It appears that with the laser and plasma conditions of this particular experiment the plasma wave is localized to islands along the direction of laser propagation [126]. Time-resolved measurements of the growth of Raman instabilities were performed using a picosecond chirped laser pulse [195]. For a short laser pulse (<10 ps), forward and 30°-Raman scattering occur at the back of the pulse. The growth of the instabilities was found to be independent of the sign of the chirp. In addition, a simple temporal model was developed and shows good agreement with the experimental results. This model also indicates that the plasma wave driven by forward Raman scattering is severely damped in the case of pulses longer than a few picoseconds. Damping by the modulational instability is compatible with the experimental results. The effect of asymmetric laser pulses on electron yield from a laser wakefield accelerator has been experimentally studied [193]. Pulses (76 fs FWHM) with a steep rise and positive chirp were found to significantly enhance the electron yield compared to pulses with a gentle rise and negative chirp. Theory and simulation show that fast-rising pulses can generate larger amplitude wakes that seed the growth of the self-modulation instability. Forward- and backward-Raman scattering and the emission of fast electrons indicate that intense electron heating is likely to play a major role in the temporal growth or inhibition of the instabilities [194].

The resonant wakefield has been characterized by temporal interferometry [127, 128]. However this was done only for the tight-focusing case in which the laser spotsize is much smaller than the plasma wave wavelength ($r_l \ll \lambda_p$) and thus the transverse wakefield was much greater than the longitudinal wakefield.

The inverse free-electron laser mechanism has been invoked to explain the observation of accelerated electrons with 200 fs laser pulses [54]. Electron acceleration without significant Raman scattering has also been observed [129] with 30 fs laser pulses, and acceleration near the resonant condition was found to be accompanied by multiple filamentation; the latter of which was also observed with longer duration pulses [130, 198]. The emission of megaelectronvolt electron beams correlated with the abrupt transition of the propagation mode from the self-channelling to the filament structure [204]. The experimental results were explained by the stochastic direct laser acceleration model based on the random phase jump taking account of the focusing effect by the self-generated magnetic field. Electron acceleration was studied over a wide range of intensities and electron densities, from the classical laser wakefield regime to the self-modulated laser wakefield regime [129, 119]. In the latter case [119], the maximum electron energy reaches 70 MeV, increasing at lower electron densities and higher laser intensities. A total charge of 8 nC was measured. Simulation of the experiment [119] indicates that the electrons are accelerated mainly by relativistic plasma waves, and, to some extent, by direct laser acceleration. Electrons have been accelerated to an energy of 4 MeV during the ionization of a gas [199].

Free electrons were reported to be accelerated in vacuum to megaelectronvolt energies by a high-intensity subpicosecond laser pulse (10^{19} W cm^{-2}, 300 fs) [116]. A subsequent discussion has helped to clarify the model used to explain the results [131–133]. In numerical simulations [134] as well as experiments [135], megaelectronvolt energy electron beams have also been observed in the interactions of intense lasers with solid-targets and propagate in both the forward and backward directions (with respect to the direction of laser propagation direction, which can also be in the specular direction).

The effects of laser polarization on fast electron emission are studied from an aluminium target irradiated by ultrashort laser pulses [208]. Jet emission of outgoing fast electrons collimated in the polarization direction is observed for s-polarized laser irradiation; whereas for p-polarized irradiation, highly directional emission of outgoing fast electrons is found in the direction close to the normal of the target.

3.2.4. Ion acceleration and nuclear reactions. Energetic (megaelectronvolt) ions have been accelerated by electrostatic sheaths created in underdense plasmas [136, 137] when intense lasers are focused onto gaseous density targets. The charge-displacement was due to ponderomotive blow-out [136, 137]. When a helium-gas was used as the target, alpha particles were accelerated to several megaelectronvolts in the direction orthogonal to the direction of laser propagation, which is also along the direction of the maximum intensity gradient.

Several groups have reported the observation of ions originating from thin-film solid-density targets. Unlike previous long-pulse experiments, the ions were accelerated along the direction normal to the side of the target that is opposite to that upon which the laser was incident. The ions generally originate from water or hydrocarbons on the surface of the material. The acceleration results from several different mechanisms, which may be occurring simultaneously. Charge-displacement is again common to all, with the electrons being heated ponderomotively, such as by Brunel, $J \times B$ or stochastic heating. In one case, the electrostatic sheath is formed at the backside of the ionization layer formed on the side of the target upon which the laser is incident (front side) [139, 138]. In another case, the electrostatic sheath is formed by field ionization of the ion layer on the opposite side of the thin film target (back-side) [140, 141], the TNSA hypothesis. Numerical simulations show evidence for both front and back-side acceleration [148].

Evidence for a back-side origin comes from results obtained when wedge-shaped targets were used. The proton beam was observed to point in the direction normal to the back side of the target, which was not perpendicular to the front surface. On the other hand, lending support to the argument

for a front-side origin, a recent experiment was conducted in which deuterium was coated on a thin film of mylar, and a boron target was placed behind it [142]. Only when the deuterium was on the front side did the boron become activated by the reaction $^{10}B(d, n)^{11}C$.

The results of these experiments indicate that a large number of protons (10^{13} p) can be accelerated, corresponding to source current densities (10^8 A cm^{-2}) that are nine orders-of-magnitude higher than produced by cyclotrons, but with comparable transverse emittances ($\epsilon_\perp \leqslant 1.0\pi$ mm mrad). Proton energies up to 60 MeV [140, 141] have been observed in experiments at intensities exceeding 10^{20} W cm^{-2} (using the NOVA petawatt laser). The high end of the proton spectrum typically has a sharp cut-off, but, like the electrons discussed in section 3.2.3, is a continuum. In one experiment, protons were observed to be emitted in ring patterns, the radii of which depended on the proton energy, which was explained by self-generated magnetic fields [139].

When a 100 fs laser pulse at intensities above 1×10^{20} W cm^{-2} was used in an experiment to irradiate 100 μm thick foils, a proton beam of 1.4 MeV temperature with a cut-off at 6.5 MeV was produced [160]. A 3 μm thick foil produced a beam temperature of 3.2 MeV with a cut-off at 24 MeV. Recirculation of the electrons during the laser pulse accounts for the sharp drop off in proton energy when the target thickness exceeds 10–15 μm ($\sim$100 fs of recirculation time). Thinner targets allow for the protons to experience a longer acceleration time because simulations show the sheath forms at the rear of the target earlier in the interaction. In another experiment [161], using a 1 ps laser pulse at 10^{17} W cm^{-2} incident on a plastic target, it was shown that in order to maximize the energies of forward-emitted protons, the target thickness must be selected such that it is smaller than the hot electron range in the target but greater than the characteristic path length of the electron heat wave generated by the prepulse and the leading edge of the laser pulse. If the target thickness is smaller than the heat wave path length, both the maximum and the mean proton energies can be a decreasing function of laser energy.

Using liquid target technology, the generation of forward-accelerated sub-megaelectronvolt (up to 500 keV) protons from a 10 μm liquid water target at 1 kHz repetition rates was demonstrated [143]. Up to 3×10^2 protons per shot in a 40° FWHM divergence beam were observed.

The GEKKO MII CPA laser produces 25 J at 1.053 μm with 0.45 ps pulse length and intensities of 5×10^{18} W cm^{-2}. A 5 μm thick target produces 1.8×10^9 protons with a temperature of 3 MeV, and 100 μm targets generate a 2 MeV temperature [145]. A ring structure of proton emission leads the authors to the hypothesis that the protons are deflected by a toroidal magnetic field, estimated to be 1000 MG, which is associated with the hot electrons. The spectra of proton energies does not behave as having been attenuated through the target. Thus, they are assumed to have originated on the back surface. A two-dimensional PIC simulation supports this hypothesis, and shows that a strong toroidal magnetic field can be excited at the target rear side with expansion of plasmas. This is in direct conflict with earlier results [146].

At intensities of up to 10^{20} W cm^{-2}, a beam of ions with energies up to 40 MeV and 3×10^{12} protons with energies >5 MeV are observed [147]. In contradiction to an earlier paper [146], the authors claim backside acceleration, based on the observation that the number of accelerated protons is greater than that available from the front surface irradiated area. A maximum carbon energy of $\sim$7 MeV per nucleon is observed, as well as the production of the isotopes ^{34}Cl and ^{38}K. Isotopes are produced by fusion of ^{12}C and ^{27}Al, and the $^{63}Cu(p, n)^{63}Zn$ and $^{12}C(d, n)^{13}N$ reactions were used to determine proton energy spectrum and spatial extent.

A 1 ps laser pulse at 10^{17} W cm^{-2} is used to show that an increase in proton energy and current is possible when a double-layer foil target containing a high-Z layer and a low-Z hydrogen-rich layer on the back is used [149]. Proton energies and current increase with the Z of the high-Z layer and depend on the layer thicknesses. More than 10^9 forward-emitted protons of energy >100 keV have been recorded within a cone angle <3°.

Collimated jets of carbon and fluorine ions up to 5 MeV per nucleon ($\sim$100 MeV) are observed from the rear surface of thin foils irradiated with laser intensities of up to 5×10^{19} W cm^{-2} [153]. Proton acceleration was suppressed by resistive heating of targets. 10^{12} protons ($E_{max} = 25$ MeV) per shot were observed without heating, and 10^{10} ($E_{max} = 3$ MeV) after heating. Using Al targets with a deposited layer of C on the back at 600 K, the energy of the carbon atoms increased by 2.5 with heating and the number to $\sim 2 \times 10^{11}$, corresponding to a laser-to-ion energy conversion of 0.5%. Using tungsten targets at 1200 K with a layer of CaF_2 they saw F^{7+} ions with energies greater than 100 MeV.

Targets of medium and high atomic numbers were irradiated by a 1 ps laser pulse of intensity up to 5×10^{16} W cm^{-2}. Up to 1 MeV highly charged heavy ions (Ta^{38+}, Au^{33+}), as well as Ar-like Ag ions and fully striped Al ions were created [154].

The Trident laser facility (1.5 TW, >1 J, 0.6 ps, and 3×10^{19} W cm^{-2}) was used for high-resolution proton radiography of Au grids [155]. The effective proton source size affords an inherent resolution of 2–3 μm in the object plane: 100 times better than conventional sources. 5×10^9 protons per shot in the 0.2–2 MeV energy range were generated. 18 MeV protons were observed from 3 μm Al targets and 22 MeV protons from a 5 μm Au, but fewer total protons.

The VULCAN laser operated at 1.054 μm, 1 ps energy and up to 100 J was used to produce 10^{12} protons above 3 MeV per shot, with a maximum energy around 25 MeV from Al foils 3–25 μm thick at 10^{19} W cm^{-2} [156, 157]. Whole target charge-up due to the expulsion of fast electrons during the interaction was measured. The charge was estimated to be $Q = 2 \times 10^{-8}$ C. The corresponding electric field at the target surface is $E = 10^{10}$ V m^{-1}.

When VULCAN had its pulses split into two 20 J beams, one arm produced protons of 6–7 MeV from Al foils used to image a 0.3 μm CH foil irradiated at $5–7 \times 10^{19}$ W cm^{-2}. The laser in this underdense plasma can produce long-lived, macroscopic bubblelike structures, seen when the protons are deflected by the associated electric charge [157]. These structures were interpreted as the remnants of a cloud of relativistic solitons.

The production of radionuclides has been used as an ion energy diagnostic [159]. In another example of a nuclear

reaction initiated by an intense laser, neutrons have been produced by the He fusion reaction $d(d,n)^3$He in the focus of 200 mJ, 160 fs Ti : sapphire laser pulses on a deuterated polyethylene target. Optimizing the fast electron and ion generation by applying a well-defined prepulse led to an average rate of 140 neutrons per shot [162]. Also, bright x-rays from solid-target interactions have created isotopes of high-Z metals by means of photofission [163–165]. Laser-accelerated electron energies and angular distributions have been inferred from analysing (γ, n) and $(\gamma, 2n)$ reactions in composite Pb/Cu targets [117] and in Ta/Cu targets [166]. Positrons were created by colliding laser-accelerated electrons with a tungsten target [167, 192].

3.2.5. Self-generated magnetic fields. Measurements of magnetic fields generated during ultrahigh intensity (10^{19} W cm^{-2}), short pulse (0.71 ps) laser-solid target interaction experiments have been reported using Faraday rotation of either the fundamental light at the critical density [184, 34] or the higher order harmonics above critical density [185, 186]. Measurements indicate the existence of peak fields greater than 340 MG and below 460 MG at such high intensities. Magnetic fields in excess of 7 MG have been measured with high spatial and temporal precision during interactions of a circularly polarized laser pulse with an underdense helium plasma at intensities up to 10^{19} W cm^{-2} [184]. The fields, while of the form expected from the inverse Faraday effect for a cold plasma, are much larger than expected, and have a duration approaching that of the high-intensity laser pulse (<3 ps). These observations can be explained by particle-in-cell simulations in three dimension. The simulations show that the magnetic field is generated by fast electrons which spiral around the axis of the channel created by the laser field.

4. Prospects and applications

Some of the advances on the horizon in the area of theory and simulation include (1) improved three-dimensional codes; (2) massively parallel processing; (3) three-dimensional visualization; and (4) fluid/particle hybrid models. Advances in laser technology are making new physical phenomena accessible and improving the accuracy of high field measurements. For instance, the repetition rate of terawatt-class lasers has increased exponentially in the last decade, making it easier to use signal averaging to increase signal-to-noise levels. Taking full advantage of the intrinsic bandwidth of Ti : sapphire, the pulse duration of terawatt lasers is also decreasing, approaching the single-cycle limit. With adaptive optics such as deformable mirrors (a technology borrowed from astronomy), these lasers can also now be focused almost to the diffraction limit (a single wavelength) [168].

4.1. Towards higher laser intensity

Because of either imperfect compression or amplified spontaneous emission, background light accompanies the short intense pulse at the focus. Thus, as laser intensities increase, so does the need for higher laser contrast (the ratio of the peak intensity to the background light intensity). Plotted in figure 8 is the laser intensity versus time for two different laser-pulse contrasts, an ideal Gaussian shape and a typical pulse (contrast of 10^5). Also shown are the various mechanisms that occur in solid-target interactions at various intensities. The peak of a high-intensity laser pulse can be orders of magnitude above the thresholds of, and arrive significantly after, plasma creation and expansion. Under such conditions, the high intensity portion of the laser pulse will deposit its energy at the critical density of a long scalelength plasma rather than directly at solid density. In order to mitigate this problem, the laser contrast is being improved by the use of frequency doubling, saturable absorbers [169] and frequency modulators to correct for high-order phase abberations [170]. The latter technology is also permitting the generation of arbitrarily shaped pulses.

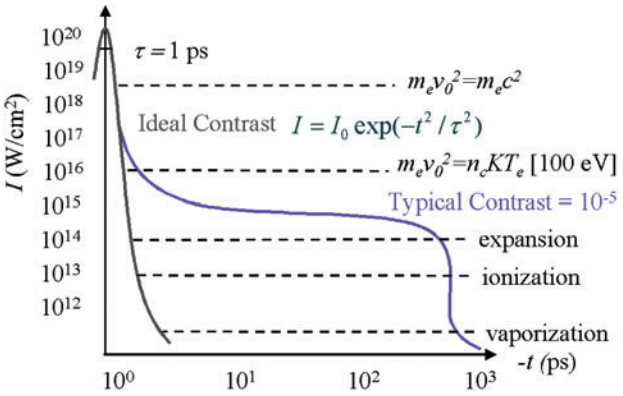

Figure 8. Laser intensity versus time for two different laser-pulse contrasts, ideal Gaussian and typical. Also shown are the various mechanisms that occur in solid–target interactions; those that occur at low intensities are initiated significantly in advance of the peak of the pulse, which corresponds to time zero. This illustrates the need for high laser contrast.

Compression and amplification of laser pulses with plasma gratings [171] might also someday increase the maximum power density of intense lasers, which in CPA systems is limited by the material damage of the final metal or dielectric grating.

4.2. Optical injection for monoenergetic beams

Proof-of-principle experiments are underway at various laboratories to use multiple synchronized laser pulses [170] to simultaneously channel-guide intense laser pulses [110–113] and coherently control wakefields [60, 61, 18] and electron injection [28–33]. The near-term milestone goal is to accelerate electrons monoenergetically up to an energy of 1 GeV in a single 1 cm long plasma channel. This could be the first stage of a multiply staged accelerator that might achieve energies relevent to high-energy physics and may also be important for applications requiring low longitudinal emittance, such as free-electron lasers.

4.3. Ultrafast studies

The production of x-rays based on the use of Thomson scattering [172, 173] will enable ultrafast imaging on the atomic scale. If the source of the electron beam were a laser accelerator, the footprint of this synchrotron-like device would be small enough to fit in a university laboratory, as discussed

theoretically [91, 88, 83] and observed experimentally [81]. Several labs have already used short-pulse incoherent x-rays generated from solid-target interactions to study time-resolved ultrafast phenomena, such as melting [174–176]. Sub-femtosecond high harmonic light from an atomic medium has been used to study inner-shell atomic transitions with 8 fs time resolution [89]. Biomedical applications of this radiation have been explored, including differential absorption and gated-viewing imaging [90]. A sufficient number of electrons have already been accelerated by laser–plasma accelerators to conduct time-resolved radio-chemistry experiments [177]. Time-resolved radio-biological studies with laser-accelerated protons are also feasible.

4.4. Relativistic ions

At the higher intensities that should be achievable in the near future ($I\lambda^2 \simeq 10^{24}\,\mathrm{W\,cm^{-2}}\mu\mathrm{m}^2$), experiments will move to the regime in which even protons begin to quiver relativistically. Predictions indicate that protons can be accelerated to relativistic velocities in plasma wakefields at much lower intensities ($I\lambda^2 \simeq 10^{21}\,\mathrm{W\,cm^{-2}}\mu\mathrm{m}^2$) [32]. At intensities exceeding $I\lambda^2 \simeq 10^{20}\,\mathrm{W\,cm^{-2}}\mu\mathrm{m}^2$, positrons will be produced more rapidly than they annihilate, making possible the creation of dense electron–positron plasmas [46]. Such exotic plasma exists at the horizons of black holes and is thus relevant to astrophysics.

4.5. Fast ignitor fusion

Evidence suggests that a laser-induced burst of hot electrons or protons could be used as a spark plug to ignite a thermonuclear reaction with inertial confinement fusion. A short but energetic (1 kJ) laser pulse would drill through the underdense plasma and a second shorter pulse would accelerate electrons of a few megaelectronvolt energy into the core. This would reduce the requirement on the usual long-pulse-duration heating and compression pulses from MJ to 100 kJ levels [178, 179]. The use of a short pulse of protons for the ignitor has also been discussed [?, 180, 181]. The energy deposition of a relativistic electron beam in a plasma can be managed through turning on or off fast beam-plasma instabilities in desirable regions [182]. This management may enable new ways of realizing the fast-igniter scenario of inertial fusion. Collisional effects alone can decelerate electrons of at most a few megaelectronvolt within the core of an inertial-fusion target. Beam-excited Langmuir turbulence, however, can decelerate even ultrarelativistic electrons in the core. Filamented transport of laser-generated relativistic electron beams in a plasma has been studied [187], based on transverse two-dimensional particle-in-cell simulation. Coalescence of current filaments and related ion dynamics are found to determine beam stopping and ion heating. Fast ignition by laser generated proton beams was studied by numerical simulation [180, 181, 158]. This analysis shows that a light ion beam triggered by a few-hundreds-kilojoule laser at intensities of $\sim 10^{21}\,\mathrm{W\,cm^{-2}}$ is relevant to the fast ignitor scenario [181]. Further study also found [158] that a capsule absorbing 635 kJ of 210 eV thermal x-rays, and a fusion yield of almost 500 MJ, could be designed, which could allow for a target gain of 200. A new compression geometry was demonstrated experimentally [188] that combines production of compressed matter in a laser-driven implosion with picosecond-fast heating by a laser pulse timed to coincide with the peak compression. This approach therefore permits efficient compression and heating to be carried out simultaneously, providing a route to efficient fusion energy production.

4.6. Proton therapy

Proton therapy is now limited by the extraordinary expense of cyclotrons or synchrotrons and the large magnets required to transport the proton beams to the patient. Currently, there are only three hospital proton therapy centres, with an additional six planned or being built. Besides reduced cost, protons are superior to other forms of ionizing radiation for cancer treatment because of less straggling and their ability to deposit their energy over a narrower depth range. But in order for a proton beam to be useful for proton therapy, the intensity should be $1\text{–}5 \times 10^{10}\,\mathrm{proton\,s^{-1}}$ with an energy of 200 MeV. Thus the repetition rate of laser-produced beams must be increased. Several ideas are being explored to improve the monochromaticity of proton beams [189].

4.7. Ion propulsion

Ions accelerated by short-pulse high-intensity lasers have several attributes that may make them advantageous for propulsion [213, 214]. Because of their relatively large momentum, they deliver a high specific impulse ($10^6\,\mathrm{s^{-1}}$) but low thrust. As such, they are attractive either for deep-space missions or for stationing orbiting satellites. Because the acceleration of ions with short duration laser pulses is relatively rapid, little energy is lost to thermal conduction as compared with ions accelerated by long-duration laser pulses.

Acknowledgments

The author acknowledges the support of the Department of Energy and the National Science Foundation. He also thanks S Banerjee, E Esarey, K Flippo, A Lapiere, Y Y Lau, R Shah, S Sepke and K TaPhouc for their valuable input.

References

[1] Maine P *et al* 1988 *IEEE J. Quant. Electron.* **24** 398
[2] Mourou G A 1997 *Appl. Phys.* B **65** 205
[3] Pogorelsky I V 1998 *AIP Conf. Proc.* **426** 415
[4] Umstadter D *et al* 1997 *IEEE J. Quant. Electron.* **33** 1878
[5] Umstadter D 2001 *Phys. Plasmas* **8** 1774
[6] Tajima *et al* 2002 *Phys. Rev. STAB* **5** 031301
[7] Esarey E *et al* 1996 *IEEE Trans. Plasma Sci.* **PS-24** 252
[8] Gibbon P *et al* 1996 *Plasma Phys. Control. Fusion* **38** 769–93
[9] Joshi C J *et al* 1995 *Phys. Today* **48** 36–43
[10] Gamiliy E G 1994 *Laser Part. Beams* **12** 185
[11] Mourou G *et al* 1992 *Phys. Fluids* B **4** 2315–25
[12] Luther-Davies B *et al* 1992 *Sov. J. Quant. Electron.* **22** 289–325
[13] Campbell E M *Phys. Fluids* B **4** 3781–99
[14] Burnett N H *et al* 1977 *Appl. Phys. Lett.* **31** 172
[15] Landau L D 1948 *Teoriia Polia* (Moscow: Nauka)
[16] Ginzburg V L 1978 *Key Problems of Physics and Astrophysics* (Moscow: Mir)
[17] Tajima T *et al* 1979 *Phys. Rev. Lett.* **43** 267
[18] Umstadter D *et al* 1994 *Phys. Rev. Lett.* **72** 1224
[19] Antonsen T M Jr *et al* 1992 *Phys. Rev. Lett.* **69** 2204

[20] Andreev N E *et al* 1992 *JETP Lett.* **55** 571
[21] Sprangle P *et al* 1992 *Phys. Rev. Lett.* **69** 2200
[22] Rosenzweig J B *et al* 1988 *Phys. Rev. Lett.* **61** 98
[23] Kitagawa Y *et al* 1992 *Phys. Rev. Lett.* **68** 48
[24] Bertrand P *et al* 1994 *Phys. Rev.* E **49** 5656
[25] D Umstadter *et al* 1996 *Science* **273** 472
[26] Moore C I *et al* 1997 *Phys. Rev. Lett.* **79** 3909
[27] Bulanov S V *et al* 1997 *Phys. Rev. Lett.* **78** 4205
[28] Umstadter D *et al* 1996 *Phys. Rev. Lett.* **76** 2073
[29] Esarey E *et al* 1997 *Phys. Rev. Lett.* **79** 2682
[30] Rau B *et al* 1997 *Phys. Rev. Lett.* **78** 3310
[31] Hemker R G *et al* 1998 *Phys. Rev.* E **57** 5920
[32] Bulanov S V *et al* 1999 *Plasma Phys. Rep.* **25** 701
[33] Moore C I *et al* 1999 *Phys. Rev. Lett.* **82** 1688
[34] Borghesi M *et al* 1998 *Phys. Rev. Lett.* **80** 5137
[35] Bhattacharyya B *et al* 1999 *Phys. Lett.* A **249** 324
[36] Brunel F 1987 *Phys. Rev. Lett.* **59** 52
[37] Bezzerides B *et al* 1882 *Phys. Rev. Lett.* **49** 202
[38] Liu X *et al* 1992 *Phys. Rev. Lett.* **69** 1935
[39] Kalashnikov M P *et al* 1994 *Phys. Rev. Lett.* **73** 260
[40] Wilks S C *et al* 1992 *Phys. Rev. Lett.* **69** 1383
[41] Sakharov A S *et al* 1997 *Phys. Plasma* **4** 3382
[42] Barr H C *et al* 2000 *Phys. Plasma* **7** 2604
[43] Esarey E *et al* 2000 *Phys. Rev. Lett.* **84** 3081
[44] Duda B J *et al* 2000 *Phys. Rev.* E **61** 1925
[45] Yu I *et al* 1999 *Phys. Rev. Lett.* **83** 2206
[46] Liang E P *et al* 1999 *Phys. Rev. Lett.* **81** 4887
[47] Quesnel B *et al* 1998 *Phys. Rev.* E **58** 3719
[48] Troha A L *et al* 1999 *Phys. Rev.* E **60** 926
[49] Pukhov A *et al* 1996 *Phys. Rev. Lett.* **76** 3975
[50] Pukhov A *et al* 1997 *Phys. Rev. Lett.* **79** 2686
[51] Ren C *et al* 2000 *Phys. Rev. Lett.* **85** 2124
[52] Gorbunov L *et al* 1996 *Phys. Rev. Lett.* **76** 2495
[53] Pukhov A *et al* 1999 *Phys. Plasma* **6** 2847–54
[54] Gahn C *et al* 1999 *Phys. Rev. Lett.* **83** 4772
[55] Sprangle P *et al* 2000 *Phys. Rev. Lett.* **85** 5110
[56] Ritchie B *et al* 1998 *Phys. Rev.* E **57** 4645
[57] Startsev E A *et al* 1997 *Phys. Rev.* E **55** 7527
[58] Shvets G *et al* 1996 *Phys. Plasmas* **3** 1109
[59] Tzeng K-C *et al* 1998 *Phys. Rev. Lett.* **81** 104
[60] Spitkovsky A and Chen P 2001 *AIP Conf. Proc.* **569** 183
[61] Rundquist A R *et al* 2001 *AIP Conf. Proc. No* 569, pp 177–82
[62] Decker C D *et al* 1994 *Phys. Rev.* E **50** R3338
[63] Andreev N *et al* 1996 *IEEE Trans. Plasma Sci.* **PS-24** 448
[64] Tzeng K-C *et al* 1997 *Phys. Rev. Lett.* **79** 5258
[65] Esarey E *et al* 1998 *Phys. Rev. Lett.* **80** 5552
[66] Wilks S *et al* 1987 *IEEE Trans. Plasma Sci.* **PS-15** 210
[67] Mora P 1992 *J. Appl. Phys.* **71** 2087
[68] Ruhl H 2001 *Plasma Phys. Rep.* **27** 363–71 (Transl. 2001 *Fizika-Plazmy* **27** 387–96)
[69] Wilks S *et al* 2000 *Phys. Plasmas* **8** 2 542
[70] Bulanov S V *et al* 2000 *JETP Lett.* **71** 407
[71] Sheng Z *et al* 2001 *Phys. Rev. Lett.* **85** 5340
[72] Gibbon P 1996 *Phys. Rev. Lett.* **76** 50
[73] Yu W *et al* 1998 *Phys. Rev.* E **57** R2531
[74] Lichters R *et al* 1996 **3** 3425
[75] Tushentsov M *et al* 2001 *Phys. Rev. Lett.* **87** 275002
[76] Naumova N M *et al* 2001 *Phys. Rev. Lett.* **87** 185004
[77] Farina D and Bulanov S V 2001 *Phys. Rev. Lett.* **86** 5289
[78] Moore C I *et al* 1995 *Phys. Rev. Lett.* **74** 2439
[79] Chen S-Y *et al* 1998 *Phys. Rev. Lett.* **80** 2610
[80] Chen S-Y *et al* 2000 *Phys. Rev. Lett.* **84** 5528
[81] Banerjee S *et al* 2003 *JOSA* B **20** 182–90
[82] He F *et al* 2002 *Phys. Plasmas* **9** 4325
[83] He F *et al* 2003 *Phys. Rev. Lett.* **90** 055002-1
[84] Park Q-H *et al* 2002 *IEEE J. Quant. Electron.* **8** 413–17
[85] Kaplan A E *et al* 2002 *Phys. Rev. Lett.* **88** 074801
[86] Christov I *et al* 1998 *Opt. Commun.* **148** 75
[87] Rax J M *et al* 1993 *IEEE Trans. Plasma Sci.* **21** 105
[88] Li Y *et al* 2002 *Phys. Rev. ST Accel. Beams* **5** 044701
[89] Drescher M 2002 *Nature* **419** 803
[90] Svanberg S 2001 *Meas. Sci. Technol.* **12** 1777–83
[91] Catravas P *et al* 2001 *Meas. Sci. Technol.* **12** 1828
[92] Takahashi E *et al* 2002 *Phys. Rev.* E **65** 016402
[93] Ueshima Y 1999 *Laser Part. Beams* **17** 45
[94] Parashar J 1997 *Plasma Phys.* **58** 613
[95] Esarey E *et al* 1992 *Phys. Rev.* A **45** 5872
[96] Hartemann F V 2001 *Phys. Rev.* E **64** 016501
[97] Khokonov M Kh 2002 *Phys. Rev. Lett.* **89** 094801
[98] Norreys P *et al* 1996 *Phys. Rev. Lett.* **76** 1832
[99] Grimes M *et al* 1999 *Phys. Rev. Lett.* **82** 4010
[100] Zhidkov A *et al* 2002 *Phys. Rev. Lett.* **88** 185002
[101] Bula C *et al* 1996 *Phys. Rev. Lett.* **76** 3116
[102] Bamber C *et al* 1999 *Phys. Rev.* D **60** 092004
[103] Borisov A B *et al* 1992 *Phys. Rev. Lett.* **68** 2309
[104] Monot P *et al* 1995 *Phys. Rev. Lett.* **74** 2953
[105] Malka G *et al* 1997 *Phys. Rev. Lett.* **79** 2053
[106] Borghesi M *et al* 1997 *Phys. Rev. Lett.* **78** 879
[107] Fuchs J *et al* 1998 *Phys. Rev. Lett.* **80** 8 1658
[108] Wagner R *et al* 1997 *Phys. Rev. Lett.* **78** 3125
[109] Krushelnick K *et al* 1997 *Phys. Rev. Lett.* **78** 4047
[110] Nikitin S P *et al* 1999 *Phys. Rev.* E **59** R3839
[111] Gaul E W *et al* 2000 *Appl. Phys. Lett.* **77** 4112
[112] Volfbeyn P *et al* 1999 *Phys. Plasmas* **6** 2269
[113] Hubbard R *et al* 1999 *AIP Conf. Proc. No* 472, pp 394–403
[114] Takahashi K *et al* 2000 *Phys. Rev. Lett.* **84** 2405
[115] Fuchs J *et al* 1998 *Phys. Rev. Lett.* **80** 2326
[116] Malka G *et al* 1997 *Phys. Rev. Lett.* **78** 3314
[117] Leemans W P *et al* 2001 *Phys. Plasmas* **8** 2510
[118] Malka V *et al* 2002 *Science* **298** 1596
[119] Malka V *et al* 2001 *Phys. Plasmas* **8** 2605
[120] Modena A *et al* 1995 *Nature* **377** 606
[121] Chen S-Y *et al* 1999 *Phys. Plasmas* **6** 4739
[122] Gordon D *et al* 1998 *Phys. Rev. Lett.* **80** 2133
[123] Ting A *et al* 1996 *Phys. Rev. Lett.* **77** 5377
[124] Le Blanc S *et al* 1996 *Phys. Rev. Lett.* **77** 5381
[125] Chen S-Y *et al* 2000 *Phys. Plasmas* **7** 403
[126] Clayton C E *et al* 1998 *Phys. Rev. Lett.* **81** 100
[127] Marques J R *et al* 1996 *Phys. Rev. Lett.* **76** 3566
[128] Siders CW *et al* 1996 *Phys. Rev. Lett.* **76** 3570
[129] Wang X *et al* 2000 *Phys. Rev. Lett.* **84** 5324
[130] Young P E *et al* 1996 *Phys. Rev. Lett.* **77** 4556
[131] McDonald K T 1998 *Phys. Rev. Lett.* **80** 1350
[132] Mora P *et al* 1998 *Phys. Rev. Lett.* **80** 1351
[133] Lefebvre E *et al* 1998 *Phys. Rev. Lett.* **80** 1352
[134] Yu W *et al* 2000 *Phys. Rev. Lett.* **85** 570
[135] Kodama R *et al* 2000 *Phys. Rev. Lett.* **84** 674
[136] Sarkisov G S *et al* 1999 *Phys. Rev.* E **59** 7042
[137] Krushelnick K *et al* 1999 *Phys. Rev. Lett.* **83** 737
[138] Maksimchuk A *et al* 2000 *Phys. Rev. Lett.* **84** 4108
[139] Clark E L *et al* 2000 *Phys. Rev. Lett.* **84** 670
[140] Snavely R A *et al* 2000 *Phys. Rev. Lett.* **85** 2945
[141] Hatchett S P *et al* 2000 *Phys. Plasmas* **7** 2076
[142] Nemoto K *et al* 2001 *Appl. Phys. Lett.* **78** 595
[143] Thoss A *et al* 2002 *Superstrong Fields in Plasmas: Second Int. Conf.* (New York: AIP) pp 353–62
[144] Sjögren A *et al* 2002 *Superstrong Fields in Plasmas: Second Int. Conf.* (New York: AIP) p 119
[145] Murakami Y *et al* 2001 *Phys. Plasma* **8** 4138
[146] Zepf M *et al* 2000 *Phys. Plasma* **8** 2055
[147] Zepf M *et al* 2001 *Phys. Plasmas* **8** 2323
[148] Wilks S C *et al* 2001 *Phys. Plasmas* **8** 542
[149] Badziak J *et al* 2001 *Phys. Rev. Lett.* **87** 215001
[150] Sentuko Y *et al* 2002 *Appl. Phys.* B **74** 207–15
[151] Ruhl H *et al* 2001 *Plasma Phys.* **27** 363–71
[152] Pukhov A 2001 *Phys. Rev. Lett.* **86** 3562
[153] Hegelich M *et al* 2002 *Phys. Rev. Lett.* **89** 085002
[154] Badziak J *et al* 2001 *Appl. Phys. Lett.* **79** 21
[155] Cobble J A *et al* 2002 *J. Appl. Phys.* **92** 1775
[156] Borghesi M *et al* 2002 *Phys. Rev. Lett.* **88** 135002
[157] Borghesi M *et al* 2002 *Phys. Plamas* **9** 2214
[158] Temporal M *et al* 2002 *Phys. Plasma* **9** 3098
[159] Santala M I K *et al* 2001 *Appl. Phys. Lett.* **78** 2001
[160] Mackinnon A J *et al* 2002 *Phys. Rev. Lett.* **88** 215006

[161] Badziak J *et al* 2002 *J. App. Phys.* **91** 5504
[162] Pretzler G *et al* 1998 *Phys. Rev.* E **58** 1165
[163] Cowan T E *et al* 2000 *Phys. Rev. Lett.* **84** 903
[164] Ledingham K W D *et al* 2000 *Phys. Rev. Lett.* **84** 899
[165] Umstadter D 2000 *Nature* **404** 239
[166] Santala M I K 2001 *Phys. Rev. Lett.* **86** 1227–30
[167] Gahn C *et al* 2000 *Phys. Lett.* **77** 2662
[168] Albert O *et al* 2000 *Opt. Lett.* **25** 1125
[169] Itatani J *et al* 1998 *Opt. Commun.* **148** 70
[170] Wefers M M *et al* 1995 *J. Opt. Soc. Am.* B **12** 1343–62
[171] Malkin V M *et al* 2000 *Phys. Plasmas* **7** 2232
[172] Leemans W P *et al* 1996 *Phys. Rev. Lett.* **77** 4182–5
[173] Pogorelsky I V *et al* 2000 *Phys. Rev. ST Accel Beams* **3** 090702
[174] Workman J *et al* 1997 *Appl. Phys. Lett.* **70** 312
[175] Rischel C A *et al* 1997 *Nature* **390** 490
[176] Siders C W *et al* 1999 *Science* **286** 1340
[177] Saleh N *et al* 2000 *Rev. Sci. Instrum.* **71** 2305
[178] Tabak M *et al* 1994 *Phys. Plasmas* **1** 1626
[179] Deutsch C *et al* 1996 *Phys. Rev. Lett.* **77** 2483
[180] Roth M *et al* 2001 *Phys. Rev. Lett.* **86** 436
[181] Yu V *et al* 2001 *Plasma Phys. Rep.* **27** 1017–20 (Transl. *Fizika Plazmy* **27** 1076–80)
[182] Malkin V M *et al* 2002 *Phys. Rev. Lett.* **89** 125004
[183] Tatarakis M *et al* 1998 *Phys. Rev. Lett.* **81** 999
[184] Najmudin Z *et al* 2001 *Phys. Rev. Lett.* **87** 215004
[185] Tatarakis M *et al* 2002 *Nature* **415** 280
[186] Tatarakis M *et al* 2002 *Phys. Plasmas* **9** 2244
[187] Honda M *et al* 2000 *Phys. Rev. Lett.* **85** 2128
[188] Kodama R *et al* 2001 *Nature* **412** 798
[189] Bulanov S V *et al* 2002 *Plasma Phys. Rep.* **28** 453–6
[190] Faure J *et al* 2002 *Phys. Plasmas* **9** 756
[191] Faure J *et al* 2002 *Phys. Rev.* E **63** 065401
[192] Gahn C *et al* 2002 *Phys. Plasmas* **9** 987
[193] Leemans W *et al* 2002 *Phys. Rev. Lett.* **89** 174802
[194] Rousseaux C *et al* 2002 *Phys. Plasmas* **9** 4261
[195] Faure J *et al* 2000 *Phys. Plasmas* **8** 2605
[196] Giulietti D *et al* 2002 *Phys. Plasmas* **9** 3655
[197] Sprangle P *et al* 2002 *Phys. Plasmas* **9** 2364
[198] Moore C I *et al* 2000 *Phys. Rev.* E **61** 788
[199] Moore C I *et al* 2001 *Phys. Plasmas* **8** 2481
[200] Kaganovich D *et al* 2001 *Appl. Phys. Lett.* **9** 3175
[201] Gordon D F *et al* 2001 *Phys. Rev.* E **64** 046404
[202] Jones T G *et al* 2002 *Rev. Sci. Instrum.* **73** 2259
[203] Peñano J R *et al* 2002 *Phys. Rev.* E **66** 036402
[204] Koyama K *et al* 2002 *CP634, Science of Super Strong Field Interactions* ed K Nakajima and M Deguchi (New York: American Institute of Physics) p 296
[205] Salamin Y I *et al* 2002 *Phys. Rev. Lett.* **88** 095005
[206] Sheng Z-M *et al* 2000 *Phys. Rev. Lett.* **85** 5340
[207] Sheng Z-M *et al* 2002 *Phys. Plasmas* **9** 3147
[208] Chen L M *et al* 2001 *Phys. Rev. Lett.* **87** 225001
[209] Sheng Z-M *et al* 2002 *Phys. Rev. Lett.* **88** 055004
[210] Shvets G *et al* 2002 *Phys. Plasmas* **9** 2383
[211] Suk H *et al* 2001 *Phys. Rev. Lett.* **86** 1011
[212] Wang P X *et al* 2001 *Appl. Phys. Lett.* **78** 2253
[213] Kammash T 2002 Fundamental study of a relativistic laser-accelerated plasma thruster *1st Int. Symp. on Beamed Energy Propulsion (Huntsville, Alabama, USA, 5–7 November 2002) AIP Conf. Series* to be published
[214] Horisawa H *et al* Fundamental study of a relativistic laser-accelerated plasma thruster *1st Int. Symp. on Beamed Energy Propulsion (Huntsville, Alabama, USA, 5–7 November 2002) AIP Conf. Series* to be published